

## Ordering and phase transitions of charged particles in a classical finite two-dimensional system

Vladimir M. Bedanov\* and François M. Peeters†

*Departement Natuurkunde, Universiteit Antwerpen (UIA), Universiteitsplein 1, B-2610 Antwerpen, Belgium*

(Received 13 September 1993)

We report a Monte Carlo study of phase transitions in a finite two-dimensional (2D) system of charged classical particles which are confined by a circular parabolic or hard-wall well. The ground-state configurations are found by static energy calculations and their structures are analyzed using the Voronoi constructions. A Mendeleev table for these classical 2D-like atoms is obtained. We calculate the radial and angular components of the displacements of the particles as functions of temperature and determine the critical temperatures for the order-disorder phase transitions. The intershell rotation and intershell diffusion transitions are investigated. The results are compared with Wigner crystallization in the infinite 2D system.

### I. INTRODUCTION

In the last decade there has been considerable theoretical and experimental progress in the study of the localization of a finite number of ions or electrons into traps. These traps are created by imposing an artificial confining potential. Examples are radio-frequency traps for ions and electrons in plasma,<sup>1</sup> heavy-ion storage rings,<sup>2</sup> electrons above liquid He which can be trapped in a bubble,<sup>3</sup> and electrons in quantum dots in semiconductor structures.<sup>4</sup> Electrons above liquid He and ions in traps and in storage rings obey classical mechanics due to the low electron density in the former case and the heavy-ion mass in the latter. A special laser cooling technique<sup>5</sup> allows one to achieve very low temperatures for ions. Electrons above liquid He are intrinsically at very low temperatures. It is well known that a classical one-component plasma at low temperatures undergoes a phase transition and forms a Wigner crystal both in three and two dimensions.<sup>6-11</sup> The interesting question is whether such a phase transition also exists in a quasi-zero-dimensional system.

The purpose of this work is to present a detailed study of a classical two-dimensional system consisting of a finite number of ions or electrons which are laterally confined by parabolic or hard-wall potentials at low temperatures where Wigner crystallization occurs for unconfined infinite systems. The possible ordered structures and phase transitions for such a system are investigated. The system of heavy-ion storage rings is similar to the present one, except that there is a third degree of freedom, i.e., along the beam axis.

The equation of state and some of the ground-state configurations have been reported by Calinon *et al.*<sup>12</sup> for a finite two-dimensional (2D) Wigner model. However, most of their results are on systems with a  $\ln(1/r)$  interaction potential, while we are interested in a pure Coulomb repulsion interaction  $1/r$ . Phase transitions were not investigated.

Recently, Lozovik and co-workers<sup>13-16</sup> have considered

a system similar to ours for the case of parabolic confinement. In the present paper, we make several of their conjectures more quantitative and improve considerably on the statistics of their simulations: (1) typically we consider at least an order of magnitude more configurations for each set of parameters, and (2) we are able to consider larger systems. We found that some of the configurations proposed by Lozovik and coauthors are unstable. Furthermore, we not only consider parabolic confinement but also investigate the other extreme case of hard-wall confinement. We found that the latter system behaves differently in several aspects.

After finishing the present work we came across a recent paper by Bolton and Rössler,<sup>17</sup> who studied the same system. They considered a classical model of a Wigner crystal in a parabolic quantum dot with  $N < 40$  electrons. They concentrated on the zero temperature configurations and possible configurational degeneracies, called cluster patterns. The differences with the present paper are as follows: we consider also larger systems with  $N > 40$ , nonzero temperature and investigate the influence of the confinement potential on our results.

The paper is organized as follows. In Sec. II we describe the model, the method of calculation, and introduce the reduced units. In Sec. III the ground-state configurations are discussed for parabolic and hard-wall confinement potentials. We analyze the shell structures using the Voronoi constructions and order the present "classical atoms" into a Mendeleev-type table. Section IV is devoted to phase transitions where we present the results from Monte Carlo simulations at different temperatures and system sizes for both confining potentials. Our conclusions are presented in Sec. IV.

### II. MODEL SYSTEM

We study a model system of a finite number  $N$  of charged particles interacting through a repulsive Coulomb potential and moving in two dimensions. A confinement potential  $V_c(r)$  keeps the system together.

The Hamiltonian for such a system is given by

$$H = \sum_{i=1}^N V_c(r_i) + \frac{q^2}{\epsilon} \sum_{j>i}^N \frac{1}{|\mathbf{r}_i - \mathbf{r}_j|}, \quad (1)$$

where  $\epsilon$  is the dielectric constant of the medium, and  $r_i \equiv |\mathbf{r}_i|$  is the distance of the  $i$ th electron from the center of the confinement potential. For convenience, we will refer to our charged particles as *electrons*, keeping in mind that they can also be ions with charge  $q$  and mass  $m$ . The first term in Eq. (1) represents the confinement potential, where we considered the following two cases: (1) parabolic confinement

$$V_c(r) = \frac{1}{2} m \omega_0^2 r^2, \quad (2)$$

and (2) hard-wall confinement

$$V_c(r) = \begin{cases} 0 & \text{if } r < R_c \\ \infty & \text{if } r \geq R_c. \end{cases} \quad (3)$$

Noting that the Hamiltonian (1) obeys a scaling law when applying the parabolic confinement potential, we can express the coordinates, energy, and temperature, respectively, in the following units:

$$r_0 = (q^2/\epsilon)^{1/3} \alpha^{-1/3}, \quad (4a)$$

$$E_0 = (q^2/\epsilon)^{2/3} \alpha^{1/3}, \quad (4b)$$

$$T_0 = (q^2/\epsilon)^{2/3} \alpha^{1/3} k_B^{-1}, \quad (4c)$$

where  $\alpha = m\omega_0^2/2$  is a measure for the one-particle confinement energy and  $k_B$  is the Boltzmann constant. All the results will be given in reduced form, i.e., in dimensionless units. In such units the Hamiltonian, in the case of parabolic confinement, becomes

$$H = \sum_{i=1}^N r_i^2 + \sum_{j>i}^N \frac{1}{|\mathbf{r}_i - \mathbf{r}_j|}, \quad (5)$$

and we notice that the ground-state configurations do not depend on the value of the confinement frequency  $\omega_0$ . The confinement frequency  $\omega_0$  defines the length and temperature scale in the system. Parabolic confinement is similar to the action of a uniform neutralizing background of charges. Consequently, changing the number of electrons  $N$  will, on the average, not change the density of the system, which is determined by the strength of the confinement frequency  $\omega_0$ .

Typical values for the units, Eq. (4), are (1) for electrons above liquid helium ( $q = -e$ ,  $\epsilon = 1$ ,  $m = m_e$ ) with a typical dimple potential<sup>18</sup> such that  $\hbar\omega_0 = 0.1$  meV = 23 GHz, we find  $r_0 = 2800$  Å,  $E_0 = 5.1$  meV, and  $T_0 = 60$  K; (2) for electrons in a GaAs heterostructure with a typical quantum dot confinement<sup>4</sup> energy of  $\hbar\omega_0 = 1$  meV we have  $r_0 = 630$  Å,  $E_0 = 1.7$  meV, and  $T_0 = 20$  K, and (3) for ions in optical traps ( $q = -e$ ,  $\epsilon = 1$ , and  $m/m_e = 4.2 \times 10^4$  for  $\text{Na}^+$ ) with a typical

confinement energy<sup>5,19</sup> such that  $\hbar\omega_0 = 3 \times 10^{-8}$  meV =  $2\pi \times 1$  kHz we obtained  $r_0 = 180$  μm,  $E_0 = 8$  μeV, and  $T_0 = 93$  mK.

In the case of hard-wall confinement, there is another parameter  $R_c$ , the radius of the well, which defines the length scale in the system. It turns out that it is convenient to choose the unit of length as  $r_0 = N^{-1/2} 2R_c$ , which implies that the parameter  $\alpha$  in Eqs. (4) has to be replaced by  $\alpha = (q^2/\epsilon) N^{3/2} (2R_c)^{-3}$ .

The standard Metropolis, or  $M(RT)^2$ , algorithm<sup>6</sup> for Monte Carlo simulation was used with automatic choice of maximal displacements to ensure an acceptance probability of 0.5. The initial configurations were chosen as fragments of the perfect Wigner triangular lattice with some appropriate interelectron spacing for a given number of electrons. The real ground-state configurations were then obtained during the Monte Carlo equilibration run at zero temperature. In order to check that there was a global minimum, the system was heated up and cooled down again to  $T = 0$ . To consider a larger system, an appropriate number of electrons was added with random coordinates  $x$  and  $y$  within a circle of radius  $R_N$ , and then the system was equilibrated. The ground-state configurations for systems with an arbitrary (but finite) number of electrons can be obtained in this manner.

In order to analyze local order in the system, in particular to identify mean coordination number and local density, we used the method of Voronoi constructions.<sup>20</sup> These are geometrical constructions which determine the minimum area for each particle. This area is the inner surface obtained by drawing perpendicular lines at the midpoint between the particle and all its neighbors (cf. the construction of the first Brillouin zone in solid state physics).

### III. GROUND-STATE CONFIGURATIONS

#### A. Parabolic confinement

In the case of not too large systems our computer simulations indicate, as do Lozovik's work and Ref. 17, that at low temperature the electrons are localized on shells. In Table I shell structures are presented for different numbers of electrons  $N$ . This table can be viewed as the present classical equivalent to the well-known Periodic Table of elements. It should be noted that some of them, for  $N = 1-21$  and  $N = 56-58$ , have been reported earlier by Lozovik and Pomirchy.<sup>13,14</sup> The electrons are arranged into shells with average interelectron distance which is dependent both on the radius (shell number) for a particular structure and on the total number of electrons [Fig. 1(a)]. The density increases with  $N$  but is lower for outer shells. For large systems we found that the structure of the inner shells is very close to the one of a triangular lattice. Namely, almost all those electrons are sixfold coordinated, whereas outer shells consist of lower-coordinated electrons [see Fig. 2(a) for the case  $N = 230$ ]. Thus there is a competition between two types of ordering: ordering into a triangular-lattice structure (Wigner lattice) and ordering into a shell structure. The

TABLE I. Ground-state configurations for the system with parabolic-confinement potential. Shell structures ( $N_1, N_2, \dots$ ), energies ( $E/N$ ), and percentage of sixfold-coordinated particles ( $P_6$ ).

$N$	$N_1, N_2, \dots$	$E/N$ (reduced units)	$P_6$ (%)
1	1	0.0	
2	2	0.75000	
3	3	1.31037	
4	4	1.83545	
5	5	2.33845	
6	1, 5	2.80456	0
7	1, 6	3.23897	100
8	1, 7	3.66890	0
9	2, 7	4.08813	50
10	2, 8	4.48494	100
11	3, 8	4.86467	67
12	3, 9	5.23895	100
13	4, 9	5.60114	25
14	4, 10	5.95899	60
15	5, 10	6.30758	40
16	1, 5, 10	6.64990	83
17	1, 6, 10	6.98291	71
18	1, 6, 11	7.30814	86
19	1, 6, 12	7.63197	100
20	1, 7, 12	7.94961	62
21	1, 7, 13	8.26588	75
22	2, 8, 12	8.57418	80
23	2, 8, 13	8.87765	70
24	3, 8, 13	9.17590	91
25	3, 9, 13	9.47079	83
26	3, 9, 14	9.76273	75
27	4, 9, 14	10.0509	92
28	4, 10, 14	10.3356	57
29	5, 10, 14	10.6193	60
30	5, 10, 15	10.8974	80
31	5, 11, 15	11.1739	56
32	1, 5, 11, 15	11.4466	53
33	1, 6, 11, 15	11.7157	89
34	1, 6, 12, 15	11.9827	84
35	1, 6, 12, 16	12.2469	89
36	1, 6, 12, 17	12.5109	89
37	1, 7, 12, 17	12.7719	85
38	1, 7, 13, 17	13.0305	76
39	2, 7, 13, 17	13.2881	82
40	2, 8, 13, 17	13.5423	87
41	2, 8, 14, 17	13.7940	79
42	3, 8, 14, 17	14.0440	64
43	3, 9, 14, 17	14.2915	65
44	3, 9, 14, 18	14.5375	61
45	3, 9, 15, 18	14.7819	67
46	4, 9, 15, 18	15.0256	82
47	4, 10, 15, 18	15.2664	83
48	4, 10, 15, 19	15.5057	65
49	4, 10, 15, 20	15.7447	83
50	4, 10, 16, 20	15.9810	77
51	5, 11, 16, 19	16.2159	78
52	1, 6, 11, 15, 19	16.4493	85
82	1, 6, 12, 18, 22, 23	22.9059	63
151	1, 6, 12, 18, 24, 30, 30, 30	35.3637	76
230	1, 6, 12, 18, 23, 25, 34, 37, 37, 37	47.4781	93

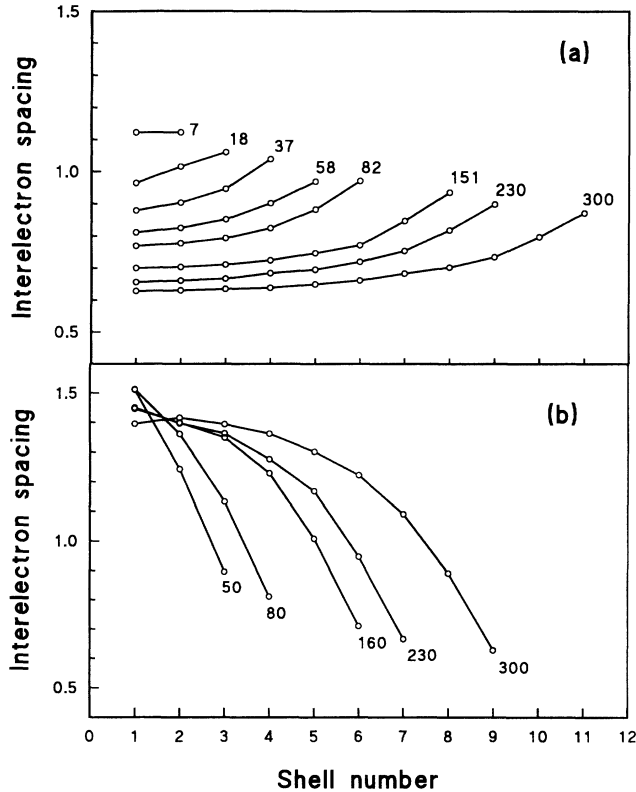


FIG. 1. Interelectron spacing as a function of shell number for different numbers of electrons  $N$  for (a) a parabolic-confinement, and (b) a hard-wall confinement potential.

triangular-lattice structure is the ordered configuration for a 2D system of point particles while the shell structure is imposed by the circular symmetry of the confinement potential. For large systems we notice that the inner electrons have a quasi-triangular-lattice structure, the outer electrons are a bend triangular lattice with equal numbers of electrons on the last few shells [Fig. 2(a) and, e.g., the largest two  $N$  values in Table I]. This is quantified in Fig. 3 where we show the radial distribution  $g(r)$  of the system of  $N = 230$  electrons measured from the center of the confinement potential. Notice that only the outer shells have a well-defined radius while the inner shells have a two peaked structure in  $g(r)$  reflecting a not well-defined shell radius because of the triangular-lattice-like structure.

When considering a sequence of systems with increasing  $N$  (see Table I), we can see how shells are being filled by electrons and sometimes a new embryo shell appears in the center. This process reminds us of the formation of the periodic system of elements. Also here there are rules for filling the shells. For instance, the first shell (counting from the center) never exceeds five electrons, and the second shell never exceeds ten electrons for  $N < 50$  and 11 for larger  $N$ . When all the shells are filled up to their maximum allowed number of electrons, a new shell, consisting of only one electron, appears in the center, when we add one electron to the system. Now the second shell has five electrons (except for  $N > 50$ ), which

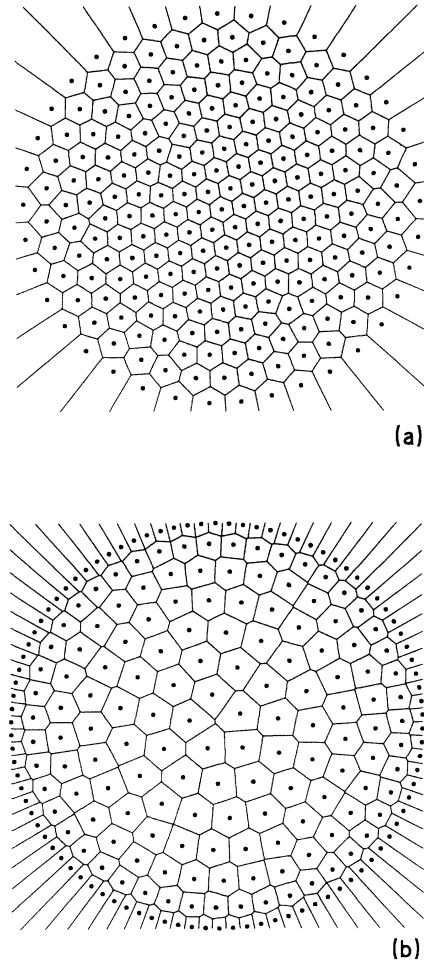


FIG. 2. Ground-state configurations and Voronoi constructions for the 230-electron system for (a) a parabolic-confinement potential, and (b) a hard-wall confinement potential.

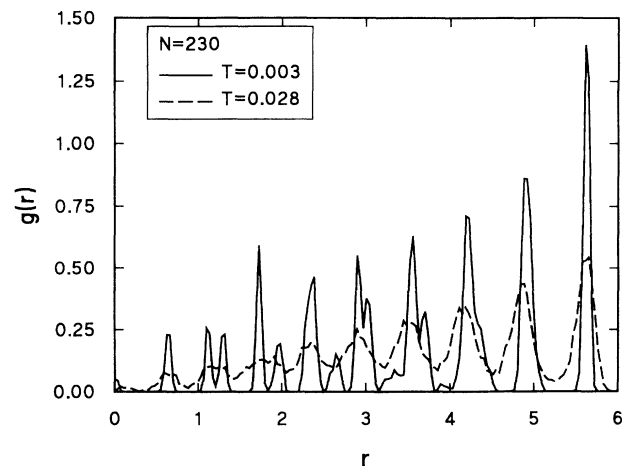


FIG. 3. The radial distribution of a system consisting of  $N = 230$  electrons in a parabolic-confinement potential for two different temperatures.

is smaller than the maximum allowed. Further adding electrons will increase the number of electrons on the different shells until each of them has reached their maximum. Rules for the number of electrons in the first shell: (1) Two electrons in the center appear only when we add one electron to the system which has the configuration (1,7,...), (2) three electrons in the center appear if we have the configuration (2,8,...), (3) four electrons if we have (3,9,...), (4) five electrons if we have (4,10,...).

It should be noted that the search of the global-minimum configurations is a difficult problem for large  $N$  values (see also Ref. 17), because of the existence of a number of local-minimum configurations, with energies very close to the global minimum. For example, in the case of  $N = 14$  the difference in energy between the global-minimum (4,10) and the local-minimum (5,9) configuration is only 0.06%. For this reason it is hard to see any nonmonotonical behavior of  $E$  versus  $N$ . Apparently, some numbers (magic numbers) allow perfect structures while others do not. Only when we plot the difference  $E(N) - E(N - 1)$  can one observe small cusps (Fig. 4) which are related to such magic numbers. The origin of these cusps can be understood from a very simple model in which we assume a constant density of electrons in each shell. Next we will find approximately the size of the systems which allow perfect shell structures. If  $d$  is the interelectron distance within a shell, which we take the same for the different shells, then the number of electrons in the  $i$ th shell is  $N_i = 2\pi R_i/d$ . For equidistant shells the radius of the  $i$ th shell is given by  $R_i = R_0 + i\Delta R$ , where  $R_0$  is the radius of the core and  $\Delta R$  is the intershell spacing. Then we have  $N_i = 2\pi R_0/d + i2\pi\Delta R/d$ . Suppose now that the local structure is close to the triangular lattice with the lattice constant  $d$ , we find  $\Delta R = \sqrt{3}d/2$ , and consequently  $N_i = 2\pi R_0/d + \pi\sqrt{3}i$  for  $i = 1, 2, \dots$ . In the following, we will take the integer part in the previous expression for each  $N_i$  and define  $N_0$  as the number of electrons in the core. Now substituting different cores with sixfold-coordinated configurations, we will obtain magic numbers for particular cores. For example, if

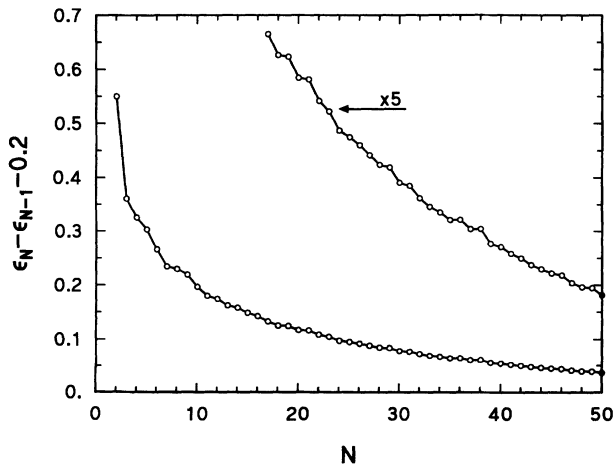


FIG. 4. The difference in ground-state configuration energies  $\epsilon_N - \epsilon_{N-1}$  as a function of the number of electrons in the system  $N$ , where  $\epsilon_N = E(N)/N$  is the energy per electron.

we choose the core consisting of one central electron and six nearest neighbors with the spacing  $d$ , i.e.,  $N_0 = 7$  and core configuration (1,6), and  $R_0 = d$  then we obtain  $N_0 = 7, N_1 = 11, N_2 = 17, N_3 = 22, \dots$ , or the set of magic numbers: 7, 18, 35, 57, . . . . For a core of two electrons we choose  $N_0 = 10(2,8)$ . In this case the second shell consists of eight electrons with the interelectron distance  $d$  and consequently  $R_0 = 8d/2\sqrt{\pi}$ . We obtained the magic numbers 10, 23, 41, . . . which are very close to the numbers in Table I with the core (2,8). For the core consisting of three electrons,  $N_0 = 3$ , we have  $R_0 = d/\sqrt{3}$  as the distance from the center of an equilateral triangle with side  $d$  to its apex. This results in the magic numbers: 12, 26, 45, . . . . Comparing these numbers and core structures with the structures presented in Table I, we observe that indeed these numbers  $N$  correspond to the inner-shell structures as we have assumed for the cores and indeed the percentage of sixfold-coordinated electrons for these  $N$  values is maximal. For large systems this simple model does not work because in this case the electron density is not uniform (see Fig. 1).

For each number  $N$  we have a particular configuration and all of them can be placed in a *periodic table*, where the *elements* from the same column exhibit similar properties. In our case this *property* is point symmetry of the inner shell. For example, there is a column of *elements* with five electrons in the center:  $N = 5, 15, 29, 30, 31, 51, \dots$

## B. Hard-wall confinement

In the case of a hard-wall confinement potential, the physical picture is more complicated. Because of the absence of a neutralizing background, electrons tend to occupy first the edge positions at the wall. This is due to the electron-electron repulsion. When a critical density at the edge is achieved, the remaining electrons form shell structures [Fig. 2(b)]. The shell structure is more pronounced here, even for large systems. However, the electron density on a particular shell now increases with increasing distance from the center [Fig. 1(b)]. For this reason our simple model does not work here and the shell structures are different than in the case of parabolic confinement. For example, for  $N = 50$  the ground-state configuration is (1, 5, 13, 31), which is quite different from the shell structure found in the case of a parabolic potential (see Table I) with 50 electrons (4, 10, 16, 20). Even when we exclude the outer-shell electrons (31 in number and thus  $N = 19$ ), we still obtain, for parabolic confinement, a very different structure (1, 6, 12). This observation should also be obvious from Fig. 1(b).

## IV. PHASE TRANSITION

After the ground configuration was achieved, the system was heated up by an amount  $\Delta T$ , typically  $1.6 \times 10^{-3}$ , and equilibrated at this new temperature during  $10^4 - 5 \times 10^4$  Monte Carlo steps. Then we calculated the mean potential energy  $U = \langle H \rangle$  the radial deviations

$$\langle u_R^2 \rangle \equiv \frac{1}{N} \sum_{i=1}^N (\langle r_i^2 \rangle - \langle r_i \rangle^2) / a^2, \quad (6)$$

and the relative angular intrashell

$$\langle u_{a1}^2 \rangle \equiv \frac{1}{N} \sum_{i=1}^N [(\langle \varphi_i - \varphi_{i_1} \rangle^2) - \langle \varphi_i - \varphi_{i_1} \rangle^2] / \varphi_0^2, \quad (7)$$

and intershell

$$\langle u_{a2}^2 \rangle \equiv \frac{1}{N} \sum_{i=1}^N [(\langle \varphi_i - \varphi_{i_2} \rangle^2) - \langle \varphi_i - \varphi_{i_2} \rangle^2] / \varphi_0^2, \quad (8)$$

square deviations, where  $i_1$  indicates the nearest parti-

cle from the same shell, while  $i_2$  refers to the nearest-neighbor shell. We introduced  $a = (\pi n)^{-1/2}$  as the average distance between the electrons with  $n$  the local electron density,  $2\varphi_0 = 2\pi/N_R$  the angular interelectron distance for the shell consisting of  $N_R$  electrons, and  $\langle \rangle$  denotes an average over the different Monte Carlo configurations, which were typically about  $10^6$ . Only relative angular displacements are considered, because we found that the system can rotate freely as a whole.

### A. Parabolic confinement

Figures 5(a)–5(d) show typical electron trajectories during Monte Carlo runs for a system of  $N = 26$  [Figs.

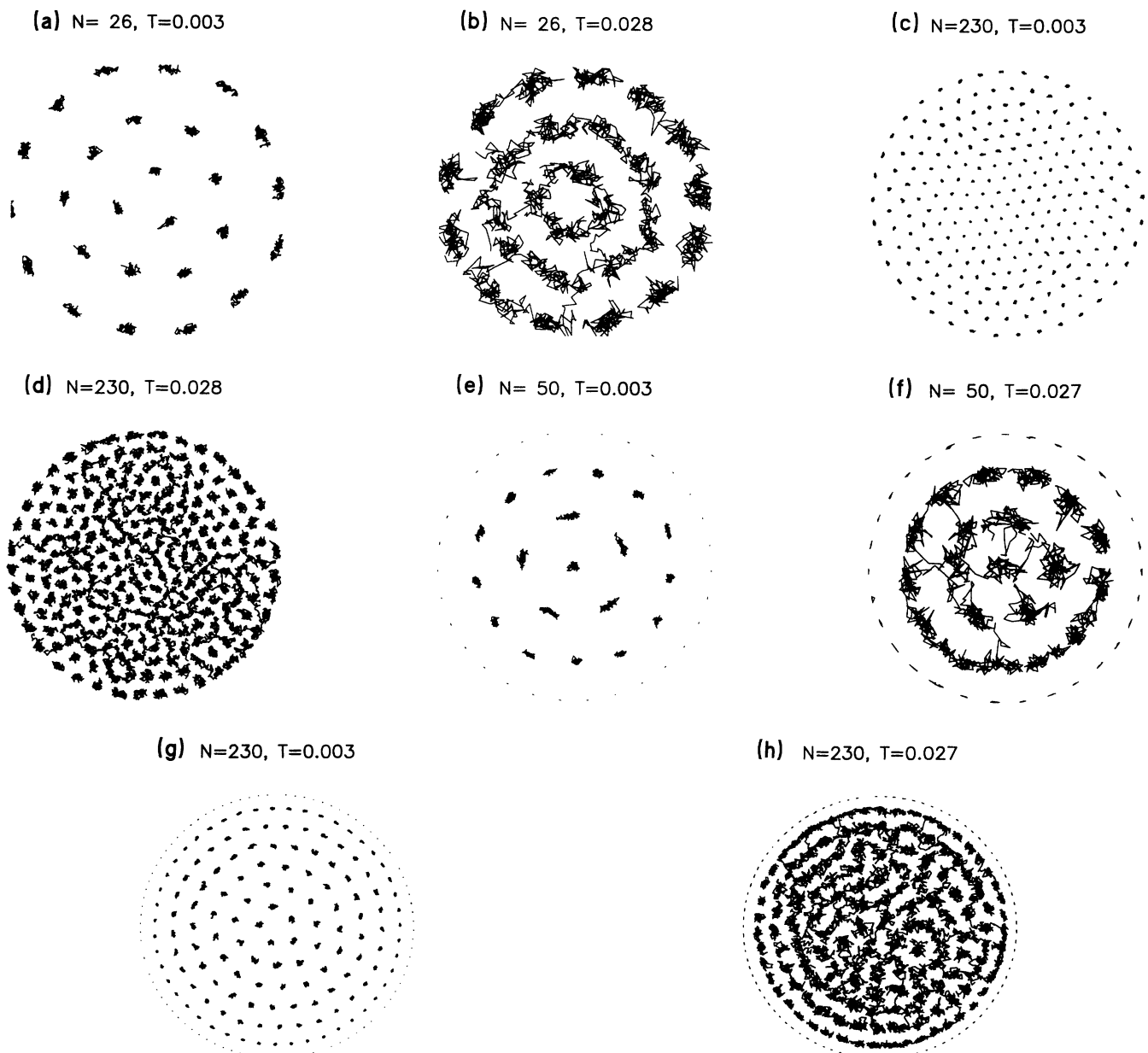


FIG. 5. Electron trajectories during 1000 Monte Carlo steps for (a)–(d) parabolic-confinement, and (e)–(h) hard-wall confinement potentials. Results are shown for different numbers of electrons and for different temperatures.

5(a) and 5(b)] and  $N = 230$  [Figs. 5(c) and 5(d)] electrons in a parabolic confinement potential. At low temperatures, electrons are well localized around their equilibrium position and the deviations from these positions are small compared to interelectron distances. However, a closer inspection shows that the displacements are anisotropic. Namely, the angular component is typically larger for small systems and also for the outer shells in a large system. At high temperatures, electrons exhibit liquidlike behavior, they can move freely within the shells, and can hop from shell to shell. Thus there should be a temperature (or temperature interval) where the system changes their behavior.

Temperature dependencies of radial and angular displacements are presented in Fig. 6 for small  $N = 26$  [Fig. 6(a)] and large  $N = 230$  [Fig. 6(b)] systems, for different shells. For large systems, radial and angular displacements change very rapidly at approximately the same temperature. Therefore there is no evidence for shell rotation with respect to each other in contrast to Lozovik's conjecture.<sup>13-16</sup> For small systems, on the other hand, the intershell displacements start to grow at much lower temperatures than the temperature at which the radial displacement jumps. This demonstrates the possibility of intershell rotation prior to the melting transition. From Fig. 6(b) we notice that in large systems the different shells melt at different temperatures, which is partly a consequence of the radius-dependent electron density [see Fig. 1(a)]. The outer shell has the lowest density and therefore we might expect intuitively the largest  $\langle u^2 \rangle$  and the lowest  $T_c$  for these shells. However, the largest  $\langle u^2 \rangle$  were found for medium shells [Fig. 6(b)]. We can explain this as follows: the outer electrons are affected by random fields which are created by their fluctuating neighbors mostly from the center and a regular parabolic field from the outside, while the electrons in the center are affected by fluctuating fields from all directions. So the fluctuations should be greater for the inner shells. As a result we have maximal displacements at some medium radius (Fig. 7). Another reason is that in large systems there exists an interface (i.e., lattice distortions) between the triangularlike and the circular structures [Figs. 2(a), 3, and 5(c) and 5(d)]. Maximal fluctuations occur in those interfacial shells.

Because of the small system size and density nonuniformity there is no definite melting temperature but rather a melting region. Nevertheless we can define a critical temperature  $T_c$  via the Lindemann criterion for melting. This implies that melting occurs when the mean displacements  $\langle u^2 \rangle = \langle \Delta \mathbf{r}^2 \rangle / a^2$  approach some critical value  $\gamma^c$ . Here  $a = (\pi n)^{-1/2}$  and  $n$  is the number density. For 2D crystals, however, this criterion is not universal, because  $\langle u^2 \rangle$  diverges logarithmically with the system size  $L$ . Therefore one considers relative displacements between two neighboring sites which are finite and the Lindemann-like criterion is applied to such relative displacements.<sup>21,22</sup> Phonon anharmonicity calculations<sup>21</sup> and molecular-dynamics simulations<sup>22</sup> found that the universal parameter for 2D melting is close to  $\gamma_c = 0.10$ . In our case, the fluctuations  $\langle u_{a1}^2 \rangle$  and  $\langle u_{a2}^2 \rangle$  are relative by definition. The radial displacements  $\langle u_R^2 \rangle$  are also

relative, because they are measured with respect to the center of the system. We found that at least for large systems the critical value for  $\langle u_R^2 \rangle$  and for  $\langle u_{a1}^2 \rangle$  is around 0.05 [Fig. 6(b)], and the criterion is fulfilled (it is a factor of 2 smaller because the present  $\langle u_R^2 \rangle$  and  $\langle u_{a1}^2 \rangle$  refer to only one direction in space). For small systems the critical value of  $\langle u^2 \rangle$  is lower, but displacements grow very fast after the critical point [see Fig. 6(a)]. To investigate the dependence of the critical temperature on the system size we define  $T_c$  as the temperature at which  $\langle u_R^2 \rangle + \langle u_{a1}^2 \rangle$ , averaged over all the shells, approaches 0.1.

The dependence of critical temperature on the number of electrons  $N$  is shown in Fig. 8(a). Also the result from a simple estimate for  $T_c$  is shown, which was obtained by using  $\Gamma = e^2 / ak_B T$  with the critical value for  $\Gamma = 137$ . The latter was found for a classical 2D Wigner crystal from experiments on electrons on the surface of liquid helium<sup>7</sup> and from computer simulations.<sup>8-11</sup> In these estimates we used the lowest local electron density found for each ground-state configuration. Except for very small  $N$ ,  $T_c$  lies lower than the one for 2D systems and it approaches slowly the limiting value at large  $N$ . The system turns out to be less stable against temperature fluctuations than the infinite one. The origin of such instability is the defect-rich interface between latticelike and circularlike structures where the fluctuations are maximal.

For very small systems ( $N < 26$ ), there is a sharp increase in the critical temperature, because such systems are mainly stabilized by the regular force from the confinement potential which dominates over the random forces created by the neighboring electrons. As a consequence the effective temperature fluctuations are smaller and the melting temperature  $T_c$  is enhanced.

It should be noted that although we plot a single point for each  $N$  in Fig. 8, there is a temperature interval  $\Delta T$ , where the transition occurs. Furthermore there are different  $T_c$  for the different shells. For  $N = 26$  this interval is small  $\Delta T = 0.001$  [see Fig. 6(a)]. However, for  $N = 230$  [see Fig. 6(b)] it is  $\Delta T = 0.005$  which is almost 50% of  $T_c$ .

## B. Hard-wall confinement

In the case of a hard-wall confinement potential, the electron density depends strongly on the shell radius [Figs. 1(b) and 2(b)]. The outer-shell electrons are practically frozen [Figs. 5(e)-5(h)] against the sharp and hard potential wall. They are pressed against the wall and can move only along the perimeter. The radial displacements for those electrons and for the inner ones differ by several orders of magnitude. Thus when analyzing transitions in such a system we did not consider the outer-electron contribution to the fluctuations. Notice that the number of such electrons at the edge is a considerable part of the total  $N$ . For example, for  $N = 50$  there are 31 electrons at the edge, and 92 electrons for  $N = 230$ . Thus in the case of hard-wall confinement we should in fact exclude these electrons such that effectively we are dealing with a smaller number of electrons.

Due to the radius-dependent electron density the fluctuations also depend strongly on the distance from the center of the well. However, in this case the dependence is monotonic. The critical temperatures for the different shells lie in a wide temperature interval  $\Delta T = 0.007$

[Fig. 6(c)]. Circular ordering dominates here even for large systems. This causes an easier rotation of shells with respect to each other. The intershell angular displacements jump at very low temperatures even for large-radius shells [Fig. 6(c)].

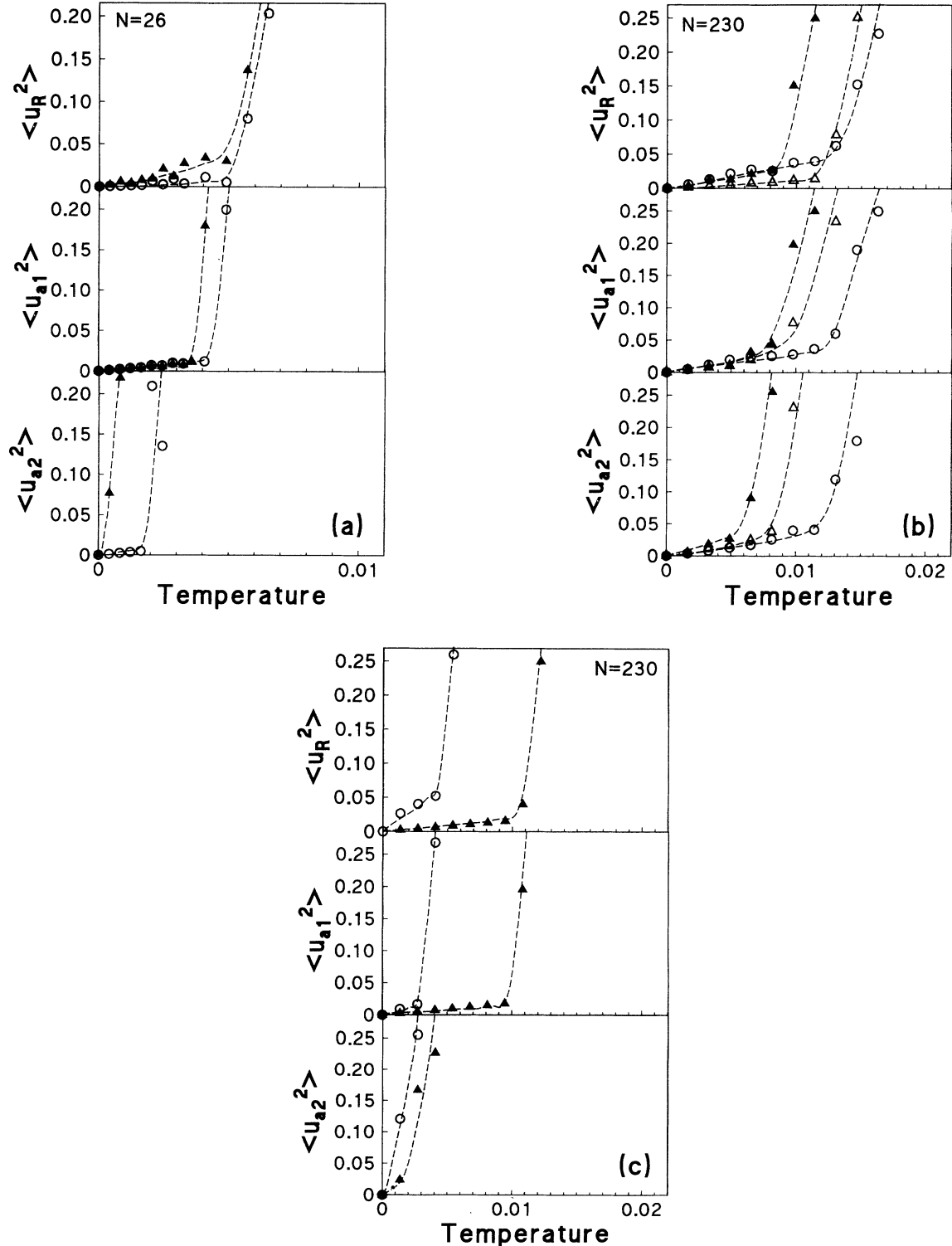


FIG. 6. Radial displacements ( $u_R^2$ ), relative intrashell ( $u_{a1}^2$ ) and intershell ( $u_{a2}^2$ ) angular displacements versus temperature for (a), (b) parabolic-confinement potential, and (c) hard-wall confinement. Results are shown for the first shell (circles), the outer shell [solid triangles (a), (c) and open triangles (b)], and the sixth shell [solid triangles (b)].

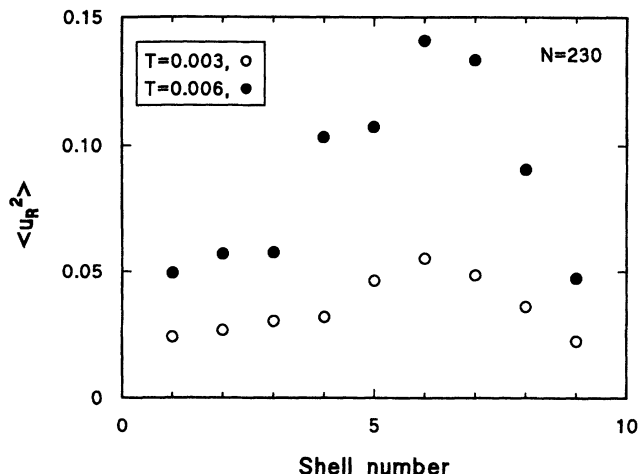


FIG. 7. Radial displacements as functions of radius (i.e., the shell number) for  $N = 230$  electrons confined in a parabolic well. Results are shown for two different temperatures. The maximal displacements are found in the sixth shell.

The critical temperature as obtained after averaging over the different shells (excluding the outer shell) is presented in Fig. 8(b) as a function of the number of electrons  $N$ . The confinement radius  $R_c$  of the well was chosen such that the average electron density  $n = N/\pi R_c^2$  was constant. The estimated critical temperatures, using  $\Gamma_c = 137$  and the minimal local electron densities (solid line), coincide with the Monte Carlo results for  $N > 50$ . The estimate using an average electron density  $n = N/\pi R_c^2$  is also shown (dotted line), which apparently overestimates  $T_c$ . Very small systems ( $N < 50$ ) again are more stable than large and infinite 2D systems.

## V. CONCLUSION

We have presented the results of a static energy calculation and of Monte Carlo simulations of a classical 2D system of point charges with parabolic and hard-wall confinement potentials. The ground-state configurations have been found. Large systems ( $N > 200$ ) with parabolic confinement exhibit almost perfect triangular-lattice structure for the inner part and circular structure for the outer one. The density of electrons is nearly constant inside and decreases slightly with radius for the outer shells. Small systems have a very clear shell structure. A Mendeleev-type table for such structures was made. In the case of hard-wall confinement the density increases with radius and electrons are arranged into well pronounced shells even for large systems.

We have studied phase transitions in such systems. Shell-structured systems undergo two-step phase transitions, both for hard-wall and parabolic confinement, as

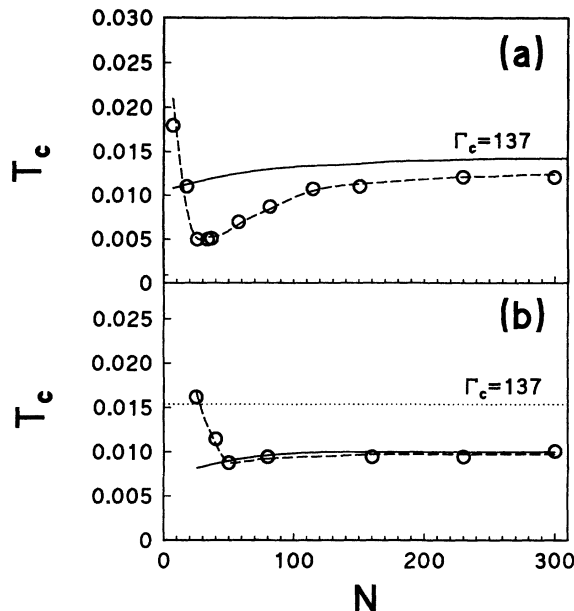


FIG. 8. Critical temperature as a function of the number of electrons  $N$  for (a) parabolic-confinement, and (b) hard-wall confinement. The solid curve corresponds to  $T_c$  as estimated through  $\Gamma_c = 137$  using the lowest electron density shell for each ground-state configuration. The dotted line in (b) is a similar estimate using the average density of the system.

reported earlier by Lozovik and co-workers<sup>13-16</sup> for the case of small systems with parabolic confinement. The first transition corresponds to intershell rotations, while the second one corresponds to intershell diffusion. Large systems with parabolic confinement behave more like infinite 2D systems, and no rotations of the shells are observed in the ordered state.

In the case of a hard-wall confinement potential, the electron density depends on the radius, i.e., the shell number, and consequently also the critical temperatures will depend on the radius. The lowest  $T_c$  is found for the inner shell, while in the case of parabolic confinement the lowest  $T_c$  was found for some intermediate shells. The latter was a consequence of the increased fluctuations at the interface between latticelike and circularlike structures which are found at some intermediate radius.

Except for very small  $N$  systems we found that the present systems are less stable against temperature fluctuations as compared to an infinite 2D system.

## ACKNOWLEDGMENTS

This work is supported by the Belgian National Science Foundation (NFWO) and the Interuniversity Microelectronics Center (IMEC, Leuven). We would like to thank F. Bolton for communicating to us the configuration  $N = 19, 23, 31, 36, 38$  in Table I.

\* Permanent address: Institute of Theoretical and Applied Mechanics, Russian Academy of Sciences, Novosibirsk 630090, Russia.

† To whom correspondence should be addressed. Electronic

address: peeters@nats.uia.ac.be

<sup>1</sup> P.E. Toschek, in *New Trends in Atomic Physics*, Les Houches, Session 38, edited by G. Grynberg and R. Stora (North-Holland, Amsterdam, 1984), Vol. 1, p. 383.

- <sup>2</sup> A. Rahman and J.P. Schiffer, in *Condensed Matter Theories*, edited by P. Vashishta, R.K. Kalia, and R.F. Bishop (Plenum, New York, 1987), Vol. 2, p. 33.
- <sup>3</sup> U. Albrecht and P. Leiderer, *Can. J. Phys.* **65**, 1536 (1987).
- <sup>4</sup> *Nanostructure Physics and Fabrication*, edited by M.A. Reed and W.P. Kirk (Academic, Boston, 1989).
- <sup>5</sup> D.J. Wineland and W.M. Itano, *Phys. Today* **40**(6), 34 (1987); C.N. Cohen-Tannoudji and W.D. Phillips, *ibid.* **43**(10), 33 (1990).
- <sup>6</sup> N. Metropolis, A.W. Rosenbluth, M.N. Rosenbluth, A.M. Teller, and E. Teller, *J. Chem. Phys.* **21**, 1087 (1953).
- <sup>7</sup> C.C. Grimes and G. Adams, *Phys. Rev. Lett.* **42**, 795 (1979).
- <sup>8</sup> R.C. Gann, S. Chakravarty, and G.V. Chester, *Phys. Rev. B* **20**, 326 (1979).
- <sup>9</sup> R.H. Morf, *Phys. Rev. Lett.* **43**, 931 (1979).
- <sup>10</sup> R.K. Kalia, P. Vashishta, and S.W. de Leeuw, *Phys. Rev. B* **23**, 4794 (1981).
- <sup>11</sup> V.M. Bedanov, G.V. Gadiyak, and Yu.E. Lozovik, *Zh. Eksp. Teor. Fiz.* **88**, 1622 (1984) [*Sov. Phys. JETP* **61**, 967 (1985)].
- <sup>12</sup> R. Calinon, Ph. Choquard, E. Jamin, and M. Navet, in *Ordering in Two Dimensions*, edited by S.K. Sinha (Elsevier, New York, 1980), p. 317.
- <sup>13</sup> Yu.E. Lozovik, *Usp. Fiz. Nauk* **153**, 356 (1987) [*Sov. Phys. Usp.* **30**, 912 (1987)].
- <sup>14</sup> Yu.E. Lozovik and L.M. Pomirchy, *Phys. Status Solidi B* **161**, K11 (1990).
- <sup>15</sup> Yu.E. Lozovik and V.A. Mandelshtam, *Phys. Lett. A* **145**, 269 (1990).
- <sup>16</sup> Yu.E. Lozovik and V.A. Mandelshtam, *Phys. Lett. A* **165**, 469 (1992).
- <sup>17</sup> F. Bolton and U. Rössler, *Superlatt. Microstruct.* **13**, 139 (1993).
- <sup>18</sup> B. Lehdorff, J. Löhle, and K. Dransfeld, *Surf. Sci.* **229**, 362 (1990); V.B. Shikin and E.V. Lebedeva, *Pis'ma Zh. Eksp. Teor. Fiz.* **57**, 126 (1993) [*JETP Lett.* **57**, 135 (1993)].
- <sup>19</sup> W. Neuhauser, M. Hohenstatt, P.E. Toschek, and H. Dehmelt, *Phys. Rev. A* **22**, 1137 (1980).
- <sup>20</sup> S. Fortune, *Algorithmica* **2**, 153 (1987).
- <sup>21</sup> Yu.E. Lozovik and V.M. Fartzdinov, *Solid State Commun.* **54**, 725 (1985).
- <sup>22</sup> V.M. Bedanov, G.V. Gadiyak, and Yu.E. Lozovik, *Phys. Lett.* **109A**, 289 (1985).